Hindawi
Mathematical Problems in Engineering
Volume 2022, Article ID 7584489, 15 pages
https://doi.org/10.1155/2022/7584489

Research Article

Model Predictive Control-Based Collision Avoidance for Autonomous Surface Vehicles in Congested Inland Waters

Wei Yuan and Pengcheng Gao

College of Electronic Information, Jiangsu University of Science and Technology, Zhenjiang 212100, China

Correspondence should be addressed to Wei Yuan; yuanwei@just.edu.cn

Received 16 March 2022; Accepted 15 April 2022; Published 30 April 2022

Academic Editor: Yuan Yang

Compared with open waters, congested inland waters have narrow waterways, many river-crossing bridges, a high density of navigation, and high current velocity in some sections. In this study, an improved collision avoidance algorithm based on model predictive control (MPC) is proposed to solve the problem of collision avoidance for autonomous surface vehicles (ASVs) in congested inland waters. First, considering the influence of current, the collision avoidance problem of ASVs is transformed into a nonlinear programming problem, and the kinematics of ASVs and the boundary of the channel are regarded as its inequality constraints. Next, since ASVs cannot perform large-scale collision avoidance in congested inland waters, the strategy of reducing the speed and slightly changing the yaw angle is adopted to realize collision avoidance. Then, an improved dynamic bumper model is used to model the safe zone of ASVs and dynamic obstacles, which improves the efficiency of the algorithm and the safety of ASVs. Finally, the collision avoidance rules and the evaluation function of the collision avoidance maneuver are constructed in the cost function of the algorithm. The simulation experiments in different encounter scenarios show that the proposed algorithm significantly improves the rationality and compliance of ASVs' autonomous collision avoidance in congested inland waters.

1. Introduction

Autonomous surface vehicles (ASVs) are intelligent robots that can autonomously navigate on the surface of the water and perform many dangerous and time-consuming tasks. In recent years, with the continuous development of computer performance [1], sensing technology [2], and artificial intelligence technology, the related technologies of ASVs have achieved rapid development and become a research focus in robotics. In addition, the strong demand from business, scientific research, and environmental protection has further promoted the application of ASVs in cargo transportation, exploration of marine resources, ecological monitoring, and other fields [3, 4]. Compared with the application of ASVs in open waters of the sea, the application of ASVs in congested inland waters is more closely related to people's daily life, which has a broader application prospect [4]. However, due to the narrow bending of the congested inland waters, many river-crossing bridges, high density of navigation, and high current velocity in some river sections, the autonomous navigation of ASVs becomes very challenging. In addition, most of the accidents are caused by human error in congested waters [5], so how to achieve effective autonomous collision avoidance is the key to ASVs in congested inland waters.

The autonomous navigation system of ASVs is usually composed of the navigation module, the guidance module, and the control module [6]. Among them, the guidance module is used to get the collision-free path of ASVs between two different positions according to the environmental information obtained by the navigation module [7]. The guidance module of ASVs usually consists of two parts: global path planning and local path planning. Local path planning is conducted to avoid the dynamic obstacles in real time according to the local environment information around the ASV. It can be divided into two categories: the reactive algorithm and the motion planning algorithm [5, 8]. Among them, the reactive algorithm, which takes the limited information in a short time into consideration, has better real-time performance when coping with sudden changes in the environment [9]. The main reactive algorithms include the

dynamic window method [10, 11] and the artificial potential field method [12, 13]. Compared with the reactive algorithm, the motion planning algorithm, which takes more information and a longer time, can provide more optimized paths. The main motion planning algorithms include the velocity obstacle method [14, 15] and the model predictive control (MPC) method [16, 17].

Compared with other collision avoidance algorithms, MPC has the characteristics of good robustness and strong anti-interference ability. MPC can adopt a nonlinear ship model to optimize the system and compensate for external disturbances in real time, reducing the system uncertainty caused by disturbances [18]. During the receding horizon optimization of the ship, MPC can simultaneously consider multiple constraints and calculate an optimal path by predicting the movement state of obstacles [19, 20]. Moreover, the assessment of collision avoidance risk, the limitations of the ship, and the navigation objectives can also be formalized in the cost function of the MPC algorithm [17]. Although there were defects in real time for MPC, its performance has been greatly improved in recent years, with the progress of computer performance, the improvement of algorithm structure, and the optimization of computing tools. The MPC algorithm has been widely applied to the path planning of unmanned aerial vehicles [21], autonomous vehicles [22–24], and unmanned surface vehicles [25].

The MPC-based collision avoidance algorithm has made many achievements for ASVs in open waters. Eriksen et al. [26] proposed an MPC-based collision avoidance algorithm that considers the influence of the International Regulations for Preventing Collisions at Sea (COLREGs) to realize autonomous collision avoidance of both static and dynamic obstacles. In order to improve the real-time performance of the collision avoidance algorithm, Sun et al. [27] adopted the finite control set model predictive control algorithm (FCS-MPC) according to the assessment of the encounter scene and the collision risk of the ASV in open waters. The COLREGs are adopted in the algorithm as the evaluation standard to realize effective collision avoidance of various dynamic obstacles. When Hagen et al. [17] designed the MPC-based collision avoidance, they adopted the collision avoidance strategy that significantly changed the surge speed and yaw of the ASV under navigation conditions in open waters, which improved the flexibility of the ASV in collision avoidance. However, the speed and yaw of ASVs are selected from a limited number of sets, which may cause discontinuity of control. In order to reduce the risk of collision avoidance, Johansen et al. [19] used a circular area to model the safety zone of the ASV when designing the MPC-based collision avoidance system. In the collision avoidance algorithm based on nonlinear MPC, Abdelaal et al. [16] adopted an elliptical zone to model the safety zone of the ASV and dynamic obstacles. However, using a standard circular or elliptical safety zone will result in many unnecessary parts in the calculation when assessing the collision avoidance risk, which reduces the computation efficiency of the algorithm.

However, due to the relatively complicated navigation conditions, there are few studies on collision avoidance in congested inland waters. In order to solve the problem of autonomous collision avoidance of ships under the condition of narrow and curved inland rivers, Cheng [28] proposed a collision avoidance algorithm based on the genetic algorithm to realize the collision avoidance of dynamic and static obstacles. Zhang [29] proposed an improved velocity obstacle method to avoid collision for inland river ferries. However, the maneuverability constraints, collision avoidance safety zone, and inland navigation rules of ASVs in the above methods are not fully considered, and there are still certain limitations in practical applications. In order to solve the problems mentioned above and make the ASVs safely navigate in congested inland waters, an improved collision avoidance algorithm based on model predictive control is proposed. The improved algorithm can effectively avoid collision against multiple obstacles, which can comprehensively consider the influence such as current, channel boundary, the actuator constraints of ASVs, and other factors. Different from open waters, ASVs cannot perform large-scale collision avoidance in congested inland waters, the collision avoidance strategy of slightly adjusting the speed and yaw is adopted. In addition, a dynamic bumper model is used to model the safety zone of ASVs and dynamic obstacles, which improves the efficiency of collision avoidance and the navigation safety of ASVs. Finally, the collision avoidance rules and the evaluation function of the collision avoidance maneuver are added to the cost function of the algorithm to ensure the compliance and rationality of the ASV manipulation during the entire collision avoidance process.

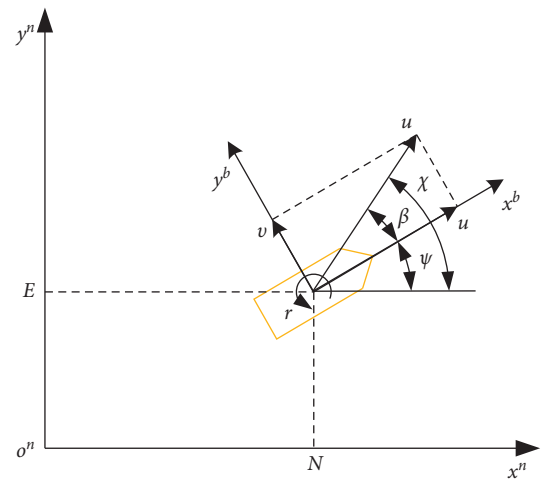

Figure 1: The Earth-fixed and body-fixed frames.

The rest of this study is organized as follows. The modeling of ASVs is given in Section 2. Section 3 provides the design of an improved collision avoidance algorithm based on MPC. In Section 4, the algorithm is verified by numerical simulation, and the result is analyzed and discussed. Finally, a summary is given in Section 5.

2. Mathematical Model of the ASV

This study takes the kinematic model of the 3DOF ASV into consideration. The motion coordinate system is shown in

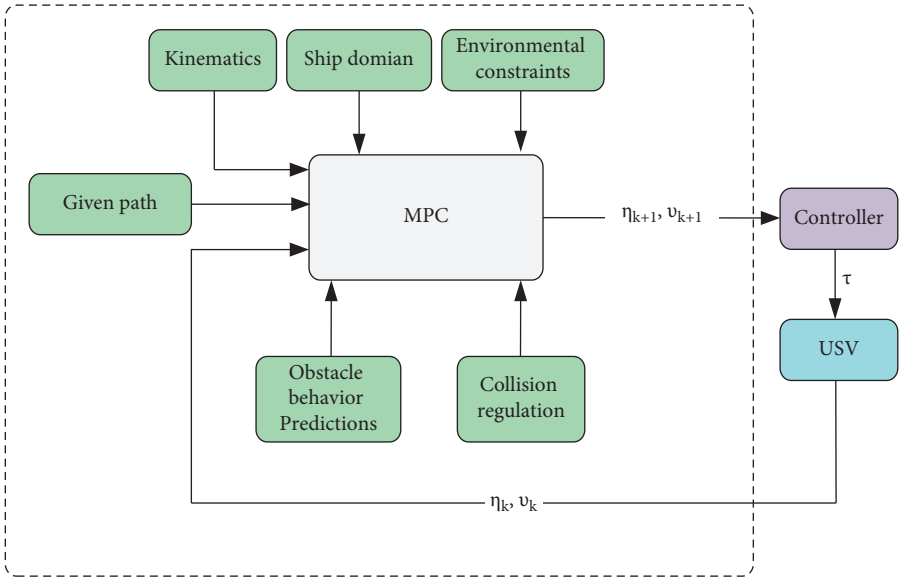

Figure 2: Block diagram of improved collision avoidance algorithm based on MPC.

Figure 1. $\eta = [x, y, \psi]^T$ and v_c, respectively, represent the pose of the ASV and current in the Earth-fixed reference frame. $v = [u, r]^T$ represents the velocity of the ASV in the body-fixed frame under the assumption of zero relative sway motion, where u is the surge speed, and r is the yaw rate of the vessel. $R(\psi)$ represents the rotation matrix from the body-fixed to the Earth-fixed frame. ψ is the yaw angle of the ship. $\chi = \psi + \beta$ is the course of the ASV. Assuming that the sideslip β of the ASV is zero, the kinematic equation of underactuated ASV can be defined as follows:

$$\begin{aligned} \dot{\eta} &= R(\psi)v + v_c, \\ \dot{\chi} &= r, \\ R(\psi) &= \begin{bmatrix} cos(\psi) & 0 \\ sin(\psi) & 0 \\ 0 & 1 \end{bmatrix}. \end{aligned} \tag{1}$$

3. Design of Improved Collision Avoidance Algorithm Based on MPC

This section presents the mathematical principle and implementation process of the improved collision avoidance algorithm. The proposed collision avoidance algorithm is shown in Figure 2.

3.1. Modeling of the Safety Zone. In this study, an improved bumper model is applied for modeling the safety zone of the ASV and obstacle ships [30]. The bumper model is obtained by statistical analysis of the vessel traffic flow data [31]. It can characterize the collision risk of the ship in the safety zone around the vessel. The bumper model is shown in Figure 3, consisting of two parts: the front and the back. The front half part is half of an ellipse; the parameters A and B represent the long and short semiaxes of the ellipse, respectively. The second half part is a semicircle with a radius of B. In order to comply with the actual navigation conditions, the size of the safety zone should vary with the velocity of the ASV or the obstacle ship [32]. As shown in Figure 4, when the surge speed of the ASV or the obstacle ship is zero, the size of the safety zone is a circular area with a radius of $B = 0.8\,L$. When the surge speed of the ASV or the obstacle ship is at its maximum, A = 5.2L and B = 0.8L in the safety zone, where L is the length of the vessel. When the surge speed of the ASV or the obstacle ship is another value, A = 0.8L + 4.4L(u/u_{max}) and B = 0.8L in the safety zone, where u_{max} is the maximum surge speed of the ASV.

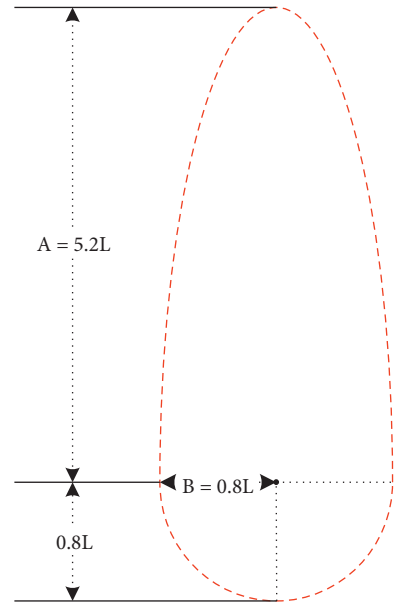

Figure 3: The bumper model.

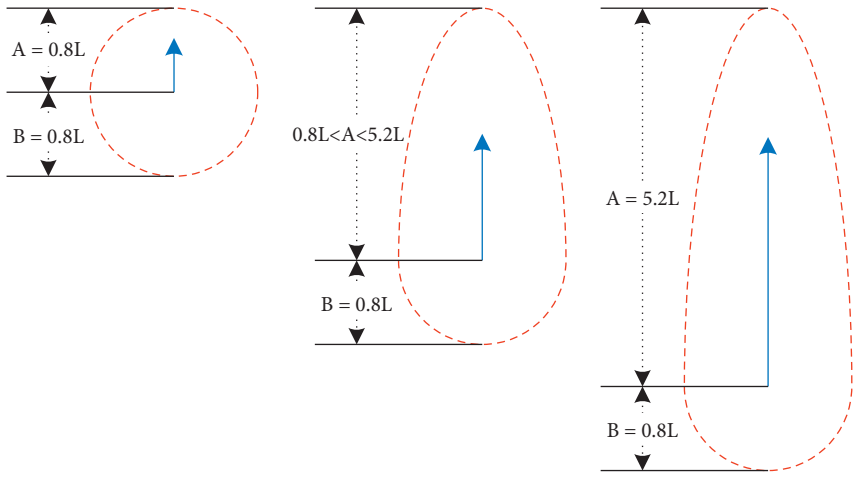

Figure 4: The dynamic safety zone. The blue arrow is the actual surge speed of ASV. (a) $u = 0$; (b) $0 \le u \le u_{\max}$; and (c) $u = u_{\max}$.

3.2. Kinematic Constraints. When ASVs navigate in congested inland waters, they can be constrained by their velocity, acceleration, and waterway's boundary, namely,

$$u_{\min} \le u \le u_{\max}, \tag{2}$$

$$r_{\min} \le r \le r_{\max}, \tag{3}$$

$$0 \le \Delta u \le \Delta u_{max}, \tag{4}$$

$$0 \le \Delta r \le \Delta r_{\max}, \tag{5}$$

$$x_{\min} \le x \le x_{\max}, \tag{6}$$

$$y_{\min} \le y \le y_{\max}. \tag{7}$$

where $u_{\min}$ represents the minimum surge speed of the ASV; $r_{\max}$ and $r_{\min}$ represent the maximum and minimum yaw rates of the ASV, respectively; Δu represents the surge speed increment of the ASV per unit time; Δr represents the yaw rate increment of the ASV per unit time; $\Delta u_{\max}$ represents the maximum surge speed increment, that is, the ASV per unit time; $\Delta r_{\max}$ represents the maximum yaw rate increment of the ASV per unit time; x_{max} and x_{min} represent the maximum and minimum values in the horizontal of the channel, respectively; $y_{\max}$ and $y_{\min}$ are the maximum and minimum values in the longitudinal direction of the channel, respectively.

Additionally, due to the limitation of congested inland waterway navigation conditions, the ASV usually adopts no more than a 40° turn when avoiding obstacles [33], namely,

$$|\psi| \le 2 * \frac{pi}{9}. \tag{8}$$

3.3. Rule Compliance. This study takes ASVs navigating in the congested waters of the Zhenjiang section of the Yangtze River as an example. ASVs must abide by the "Regulation of the People's Republic of China on Inland River Collision Avoidance" (*RPRCIRCA*) and the "Regulations on Ship Routing System in Jiangsu Section of the Yangtze River" (*RSRSJSYR*) when navigating in the waters. The most relevant rules for designing collision avoidance algorithms can be summarized as follows:

RPRCIRCA:

> Rule 9: Any actions to prevent a collision shall be taken effectively, early, and with good driving skill until the vehicle has passed.
>
> Rule 10: In a tidal stream, a lake, a reservoir, or an advection area, two vessels shall come close to meet on the port side of each other except in special circumstances.
>
> Rule 11: When a motorized vessel catches up or overtakes another motorized vessel in a direction greater than 22.5° behind its sway direction, which may pose a danger of collision, it shall be deemed overtaking.

RSRSJSYR:

> Rule 10: Vessels shall travel at a safe speed to avoid collision.
>
> Rule 12: When overtaking another vessel, a vessel shall overtake from the port side of the overtaken vessel as far as possible under the condition that safety is guaranteed.
>
> Rule 20: Any vessel that needs to cross the navigable lane or the recommended route shall pay attention to the condition of the waterway and the surrounding environment and, without hindering the safe sailing of other vessels, carry out the crossing as near as possible to the navigable lane or recommended route at a large angle.
>
> Rule 28: A vessel that fails to navigate in the prescribed navigable lane or recommended route shall take the initiative to give way to vessels that usually navigate in the defined passable lane or recommended course.

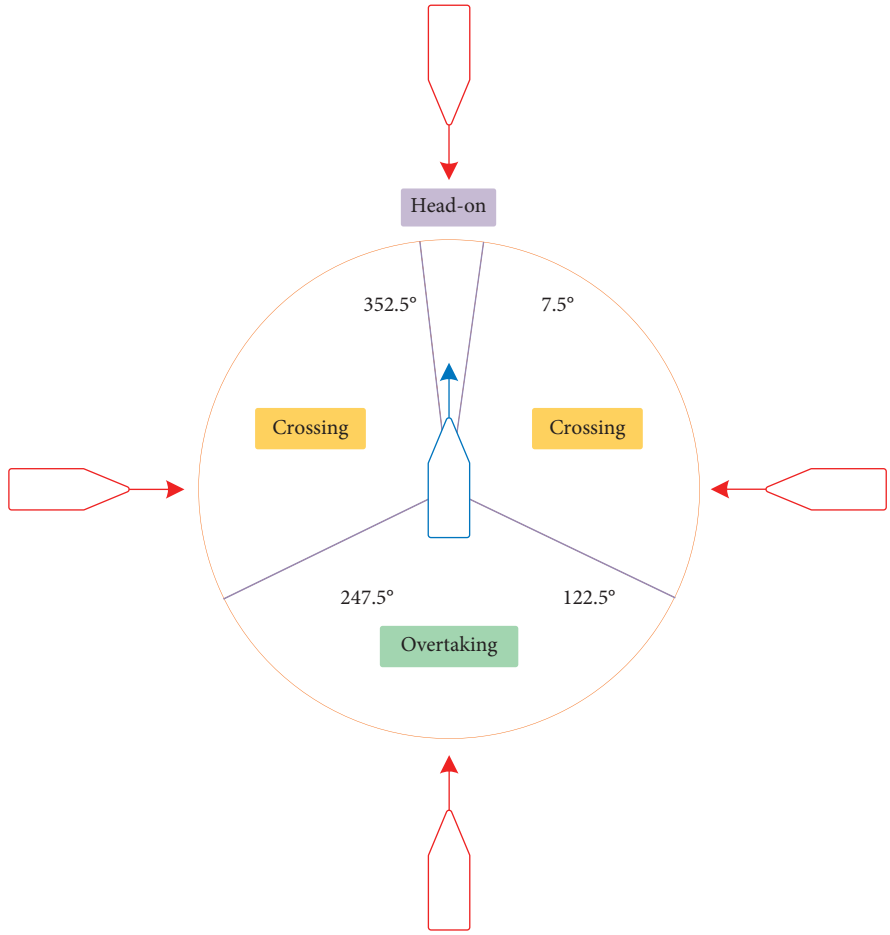

FIGURE 5: Graphic illustration is used to categorize encounters based on collision avoidance rules. The blue ship is own ASV; the red ship is an obstacle vessel.

The encounter situation between the ASV and the obstacle ship in the Zhenjiang section of the Yangtze River is mainly divided into three conditions: head-on, overtaking, and crossing. The graphic diagram of the encounter situation is shown in Figure 5. According to the requirements of the regulations, the avoidance direction of the ASV when evading an encounter scene is demonstrated in Figure 6.

3.4. Division of Encounter Situations. The primary information used to divide the encounter situation of the ASV is shown in Figure 7. The specific description is as follows:

(1) The blue ship is the ASV, and the green ship is the obstacle ship. The red dashed line represents the given path of the ASV. The blue dashed line represents the navigation path of the ASV. The green dashed line represents the navigation path of the obstacle ship.

(2) The blue vector $\overrightarrow{U}_{ow}(t)$ represents the surge speed of the ASV at time t. The green vector $\overrightarrow{U}_{obs}(t)$ represents the surge speed obstacle ship at time t. The red vector $\overrightarrow{L}(t)$ represents the unit vector of the ASV to the obstacle ship at time t.

(3) ψ represents the yaw angle of the ASV in the Earth-fixed frame at time t.

(4) At time t, when $d_{oi}(t) \le d_{\text{close}}(t)$, the obstacle ship is considered to be close to the ASV, and avoiding manipulation needs to be performed. Here, $d_{oi}(t)$ represents the Euclidean distance between the ASV and the obstacle ship at time t; $d_{\text{close}}(t)$ represents the minimum distance that the ASV needs to avoid manipulation at time t, and its size depends on factors such as the relative velocity between the ASV and the obstacle ship, the encounter situation, and environmental conditions.

When $d_{oi}(t) \le d_{\text{close}}(t)$, $|\overrightarrow{U}_{obs}(t)| \neq 0$, and

$$\begin{aligned} &\overrightarrow{U}_{ow}(t) \cdot \overrightarrow{U}_{obs}(t) < -\cos(\theta_1)\left|\overrightarrow{U}_{ow}(t)\right|\left|\overrightarrow{U}_{obs}(t)\right|, \\ &\overrightarrow{U}_{obs}(t) \cdot (\overrightarrow{L}(t)) > \cos(\theta_2)\left|\overrightarrow{U}_{obs}(t)\right|. \end{aligned} \tag{9}$$

The ASV is considered to have a head-on encounter with the obstacle ship.

When $d_{oi}(t) \le d_{\text{close}}(t)$, $|\overrightarrow{U}_{ow}(t)| > |\overrightarrow{U}_{obs}(t)|$, and

$$\overrightarrow{U}_{ow}(t) \cdot \overrightarrow{U}_{obs}(t) > \cos(\theta_3)\left|\overrightarrow{U}_{ow}(t)\right|\left|\overrightarrow{U}_{obs}(t)\right|, \tag{10}$$

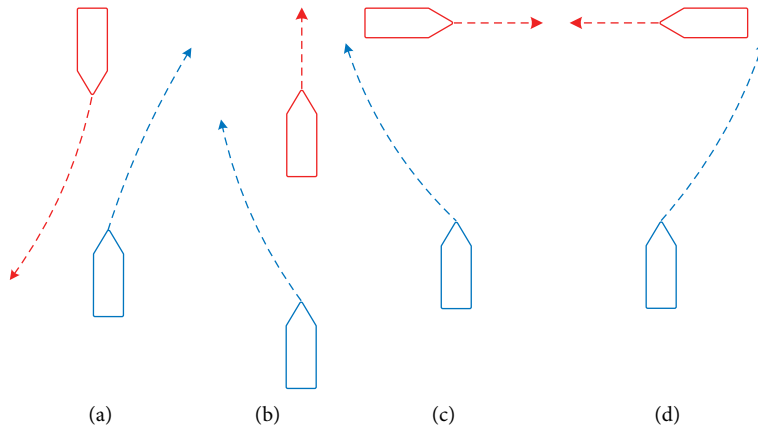

Figure 6: Avoidance direction according to collision avoidance rules. The blue ship is the ASV; the red ship is an obstacle ship. (a) Head-on; (b) overtaking; (c) crossing from port; and (d) crossing from starboard.

The ASV is behind the obstacle ship, and the ASV is considered to be overtaking the obstacle ship.

When $d_{oi}(t) \le d_{\text{close}}(t)$,

$$\vec{U}_{ow}(t) \cdot \vec{U}_{obs}(t) < \cos(\theta_4)\left|\vec{U}_{ow}(t)\right|\left|\vec{U}_{obs}(t)\right|. \tag{11}$$

The ASV is facing the obstacle ship, and the ASV is considered to be crossing the obstacle ship.

θ_1, θ_2, θ_3, and θ_4 are the angles that meet the requirements of the collision avoidance rules. The specific parameters are shown in Table 1.

3.5. Optimization Problem Construction. In this study, multiple shooting methods are applied to transform the optimal control problem of ASV collision avoidance into a nonlinear programming problem (NLP) and consider the changes in the speed and pose of the ASV during optimization. The general form of NLP is as follows:

$$\begin{aligned} &\min_{\omega} \phi(\omega), \\ &\text{s.t. } g(\omega) = 0, \\ &\quad h(\omega) \le 0. \end{aligned} \tag{12}$$

where ω represents the decision variable; $g(\omega)$ represents the equation constraint of kinematics; $h(\omega)$ represents the inequality constraint; and $\phi(\omega)$ represents the objective function. $\phi(\omega)$ is defined as follows:

$$\begin{aligned} \phi(\omega) = &\sum_{k=1}^{N_p} \left(K_p p_k - p_{d_k}^2 + K_u (u_k - u_d)^2 + K_r (r_k - r_d)\right)^2 \\ &+ \sum_{k=2}^{N_p} \left(K_{\dot{u}} * (u_k - u_{k-1})^2 + K_{\dot{r}} * (r_k - r_{k-1})^2\right) + \phi_{\text{rules}}. \end{aligned} \tag{13}$$

Among them, K_p, K_u, K_r, $K_{\dot{u}}$, and $K_{\dot{r}}$ are the adjustment parameters; p_d represents the reference path of the ASV at the sampling time k; u_d represents the reference surge speed of the ASV, r_d represents the reference yaw rate of the ASV; u_k represents the surge speed of the ASV at the sampling time k; r_k represents the yaw rate of the ASV at the sampling time k; ϕ_{rules} is the cost function used to evaluate the rule compliance for collision avoidance of the ASV; and its specific form is as follows:

$$\begin{aligned} \phi_{\text{rules}} &= \phi_{\text{heading}} \vee \phi_{\text{overtaking}} \vee \phi_{\text{crossing}}, \\ \phi_{\text{heading}} &= \sum_{k=1}^{N_p} \left(K_g \left(m * e^{r_k} + n * e^{-r_k}\right) + K_{oi}\left(i * e^{-\left(d_{oi\_z}(k) - d_{\text{safe\_heading}}\right)}\right)\right), \\ \phi_{\text{overtaking}} &= \sum_{k=1}^{N_p} \left(K_g \left(m * e^{r_k} + n * e^{-r_k}\right) + K_{oi}\left(i * e^{-\left(d_{oi}(k) - d_{\text{safe\_overtaking}}\right)}\right)\right), \\ \phi_{\text{crossing}} &= \sum_{k=1}^{N_p} \left(K_g \left(m * e^{r_k} + n * e^{-r_k}\right) + K_{oi}\left(i * e^{-\left(d_{oi}(k) - d_{\text{safe\_crossing}}\right)}\right)\right). \end{aligned} \tag{14}$$

where K_g and K_{oi} are the adjusting parameters; m, n, and i are parameters with values of 0 or 1; $d_{oi\_z}(k)$ represents the distance between the ASV and the obstacle ship in the sway direction of the ship in the Earth-fixed frame at sampling time k; $d_{\text{safe\_heading}}$, $d_{\text{safe\_overtaking}}$, and $d_{\text{safe\_crossing}}$, respectively, represent the safe distance that the ASV required to

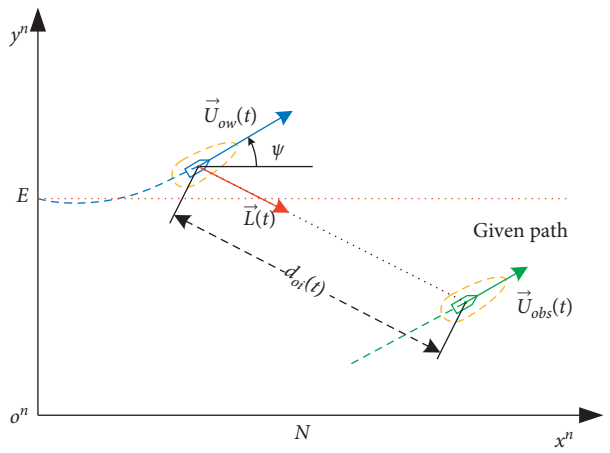

Figure 7: The primary information used to classify the encounter situation of ASVs.

Table 1: Value of θ that meets the requirements of collision avoidance rules.

Parameter	Value
θ_1	40°
θ_2	7.5°
θ_3	68.5°
θ_4	68.5°

conduct collision avoidance manipulation in the situation of head-on, overtaking, and crossing.

In NLP, the constraint of velocity and acceleration in equations (2)-(5) are defined as follows:

$$\begin{aligned} h\left(u_{1:Np}\right) &= \begin{bmatrix} u_{\min} - u_{1:Np} \\ u_{1:Np} - u_{\max} \end{bmatrix} \le 0, \\ h\left(r_{1:Np}\right) &= \begin{bmatrix} r_{\min} - r_{1:Np} \\ r_{1:Np} - r_{\max} \end{bmatrix} \le 0, \\ h\left(\Delta u_{2:\ Np}\right) &= \left[\Delta u_{2:\ Np} - \Delta u_{\max}\right] \le 0, \\ h\left(\Delta r_{2:\ Np}\right) &= \left[\Delta r_{2:\ Np} - \Delta r_{\max}\right] \le 0. \end{aligned} \tag{15}$$

where $u_{1:Np} = [u_1, u_2 \ldots, u_{Np}]$ and $r_{1:Np} = [r_1, r_2 \ldots, r_{Np}]$, respectively, represent the surge speed and yaw rate of the ASV at each NLP step. $\Delta u_{2:Np} = [u_2 - u_1, u_3 - u_2, \ldots, u_{Np} - u_{Np-1}]$ and $\Delta r_{2:Np} = [r_2 - r_1, r_3 - r_2, \ldots, r_{Np} - r_{Np-1}]$, respectively, represent the increment of the surge speed and yaw rate of the ASV at each NLP step.

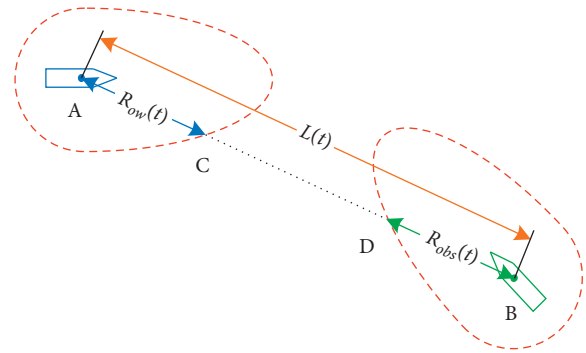

Figure 8: The obstacle avoidance principle of ASVs.

In NLP, the constraint of the waterway's boundary in equations (6) and (7) is defined as follows:

$$h\left(x_{1:Np+1}\right) = \begin{bmatrix} x_{\min} - x_{1:Np+1} \\ x_{1:Np+1} - x_{\max} \\ y_{\min} - y_{1:Np+1} \\ y_{1:Np+1} - y_{\max} \end{bmatrix} \le 0, \tag{16}$$

where $x_{1:Np+1} = [x_1, x_2 \ldots, x_{Np+1}]$ and $y_{1:Np+1} = [y_1, y_2 \ldots, y_{Np+1}]$ represent the position of the ASV at each NLP step.

In NLP, the constraints of course in equation (8) are defined as follows:

$$h_\chi\left(\chi_{1:N_{p+1}}\right) = \left[\left|\chi_{1:N_{p+1}}\right| - 2 * \frac{pi}{9}\right] \le 0, \tag{17}$$

where $\chi_{1:Np+1} = [\chi_1, \chi_2 \ldots, \chi_{Np+1}]$ represents the course of the ASV at the time related to each NLP step.

As shown in Figure 8, the position of the ASV is A, and the position of the obstacle is B in the Earth-fixed frame at time t. The intersection point of the AB connection and the safety zone of the ASV is C. The intersection point of the AB connection and the safety zone of the obstacle is D. The distance of AC is $R_{ow}(t)$, and the distance of B D is $R_{obs}(t)$. When it is a static obstacle, $R_{obs}(t)$ is a constant value. In order to ensure that the ASV effectively avoids obstacles during navigating, it must be guaranteed that, at time t, the Euclidean distance between the ASV and the obstacle is greater than or equal to the sum of AC and B D, that is, $L(t) \ge R_{ow}(t) + R_{obs}(t)$.

In NLP, in order to ensure that the ASV effectively avoids static obstacles, for a set of S static obstacles $o_s = \{o_{s1}, o_{s2}, \ldots, o_{sS}\}$, the inequality constraint is as follows:

$$h_{si}\left(L_{si}\left(t_{1:\ N_p+1}\right)\right) = \begin{bmatrix} \left(R_{si} + R_{ow}(t_1)\right) - P_{ow}(t_1) - P_{si2} \\ \left(R_{si} + R_{ow}(t_2)\right) - P_{ow}(t_2) - P_{si2} \\ \vdots \\ \left(R_{si} + R_{ow}\left(t_{Np+1}\right)\right) - P_{ow}\left(t_{Np+1}\right) - P_{si2} \end{bmatrix} \le 0, \tag{18}$$

Table 2: Parameters of the improved collision avoidance algorithm based on MPC.

Parameter	Value	Parameter	Value
L	5 m	$d_{\text{close\_crossing}}$	30 m
N	20	$d_{\text{safe\_heading}}$	20 m
T	0.1 s	$d_{\text{safe\_overing}}$	30 m
v_c	[0.3, 0.1] m/s	$d_{\text{safe\_crossing}}$	30 m
K_p	0.15	$\lvert\chi\rvert_{\max}$	$(2\pi/9)$ rad
K_u	0.7	u_{ref}	4 m/s
K_r	0.2	r_{ref}	0 rad/s
K_g	14	$[u_{\min}, u_{\max}]$	[2, 7.8] m/s
K_{oi}	0.001	$[r_{\min}, r_{\max}]$	$[-\pi/30, \pi/30]$ rad/s
$K_{\dot{u}}$	500	$\Delta u_{\max}$	1 m/s^2
$K_{\dot{r}}$	500	$\Delta r_{\max}$	$(\pi/30)$ rad/s^2
$d_{close\_heading}$	60 m	$[x_{\min}, x_{\max}]$	[0, 160] m
$d_{close\_overtaking}$	30 m	$[y_{\min}, y_{\max}]$	[0, 120] m

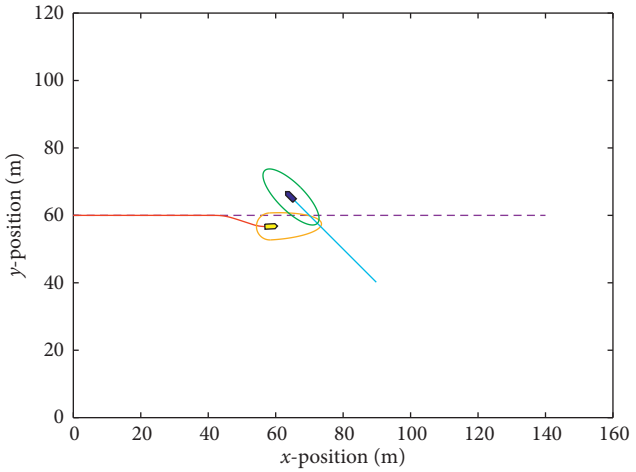

Figure 9: Collision avoidance using the standard elliptic domains.

where R_{si} represents the radius of the safety zone of the static obstacle i; $P_{ow}(t_{1:Np+1})$ is the position vector of the ASV at the sampling time $t_{1:Np+1}$; and P_{si} is the position vector of the static obstacle i.

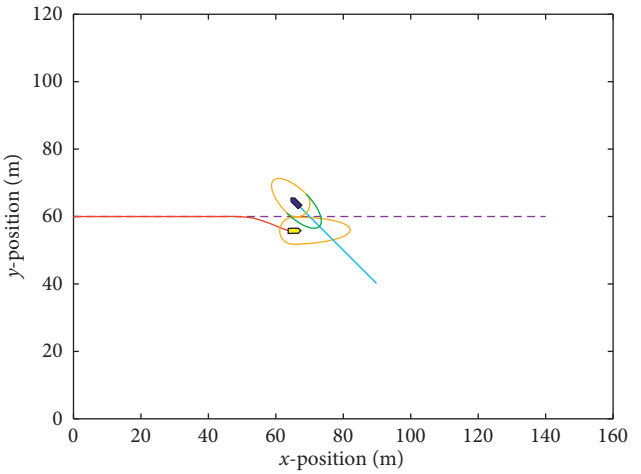

Figure 10: Collision avoidance using the dynamic bumper domain.

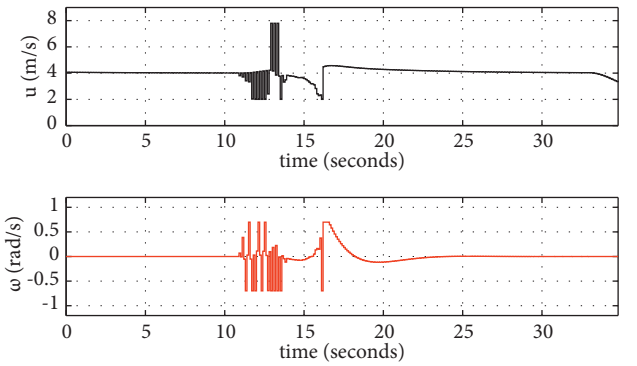

Figure 11: The surge speed and the yaw rate of the ASV during the collision avoidance using the dynamic bumper domain.

Similarly, in order to ensure that the ASV effectively avoids dynamic obstacles, for a set of M dynamic obstacle $o_m = \{o_{m1}(t), o_{m2}(t), \ldots, o_{mM}(t)\}$, the inequality constraint is as follows:

$$h\left(L_{mi}\left(t_{1:\ N_p+1}\right)\right) = \begin{bmatrix} \left(R_{mi}(t_1) + R_{ow}(t_1)\right) - P_{ow}(t_1) - P_{mi}(t_1)_2 \\ \left(R_{mi}(t_2) + R_{ow}(t_2)\right) - P_{ow}(t_2) - P_{mi}(t_2)_2 \\ \vdots \\ \left(R_{mi}\left(t_{Np}\right) + R_{ow}\left(t_{Np+1}\right)\right) - P_{ow}\left(t_{Np+1}\right) - P_{mi}\left(t_{Np+1}\right)_2 \end{bmatrix} \leq 0, \tag{19}$$

where $R_{mi}(t_{1:Np+1})$ is the value of the safety zone of the dynamic obstacles at the sampling time of $t_{1:Np+1}$; $P_{mi}(t_{1:Np+1})$ is the vector of the position of the dynamic obstacle i at the sampling time of $t_{1:Np+1}$.

4. Simulation Results and Discussion

In this section, in order to verify the performance of the proposed collision avoidance algorithm, we give the simulation results under five different situations: 1. standard ellipse domain and dynamic bumper domain; 2. head-on; 3. overtaking; 4. crossing; and 5. collision avoidance against static and dynamic obstacles.

4.1. Simulation Setup. In the simulation, we assumed that the ASV navigates in the congested waters of the Zhenjiang section of the Yangtze River, and the specific information of

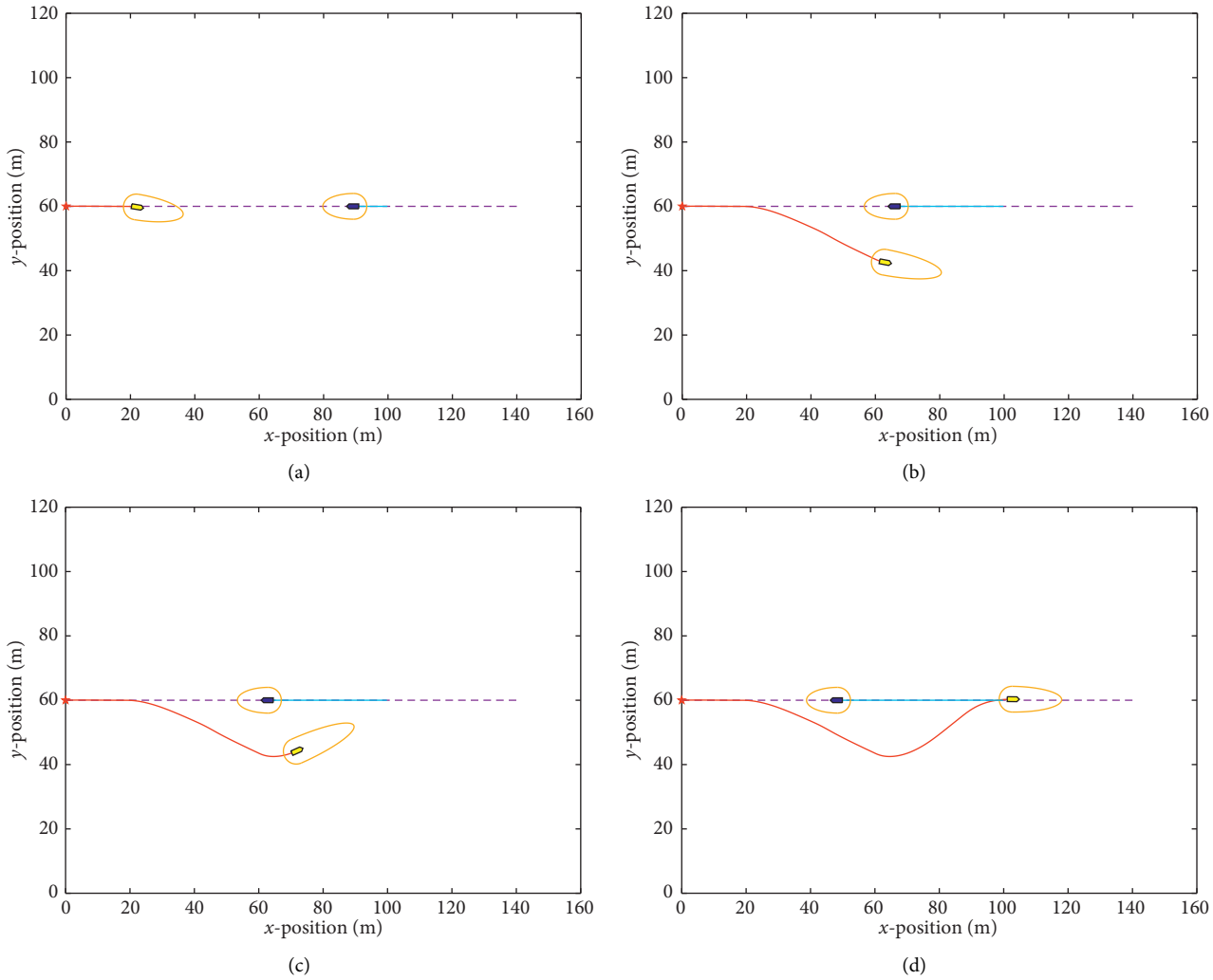

Figure 12: Simulation 2: head-on.

the obstacle ship can be known through AIS. The simulation conditions are CPU of 1.6 GHz Intel Core i5, the operating system of Window10, MATLAB R2020a, and IPOPT solver based on CASADI architecture [34]. According to the requirements of *Rule* 9 of "*RPRCIRCA*," we select the sampling time T as 0.1s and the step size N as 20 to ensure that the prediction range of the collision avoidance algorithm is significantly larger than the response time of the speed and yaw. According to the requirements of *Rule* 10 of "*RSRSJSYR*," the maximum surge speed of the ASV is set to 7.8 m/s, the minimum surge speed is set to 0 m/s in the case of crossing, and 2 m/s in other encounter scenarios. The same tuning parameters are used in all simulations, and the relevant parameters of the collision avoidance algorithm are given in Table 2.

In the simulation results, the following symbols and colors are adopted:

(1) The purple dotted line represents the given path of the ASV; the red solid line represents the navigation path of the ASV; and the light blue solid line represents the navigation path of the obstacle ship.

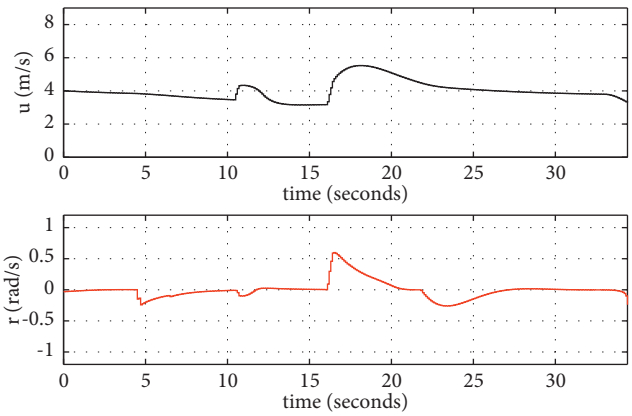

Figure 13: The surge speed and the yaw rate of the ASV during simulation 2.

(2) The golden yellow dynamic area represents the dynamic bumper domain of the ASV and obstacle ship, the dynamic green area represents the standard ellipse domain, and the blue-filled circle represents the static obstacle.

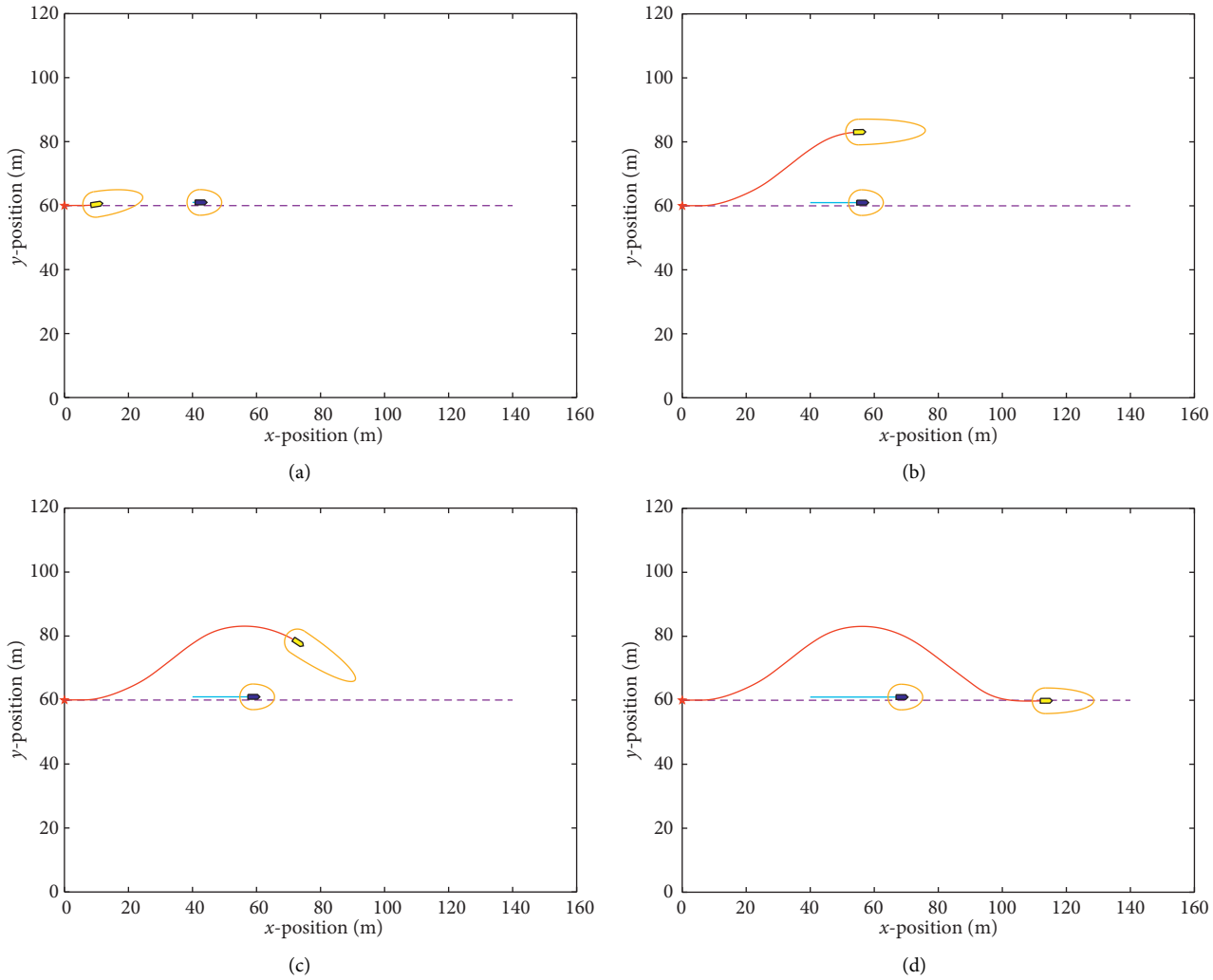

Figure 14: Simulation 3: overtaking.

(3) The yellow ship represents the ASV, and the blue ship represents the obstacle ship.

4.2. Simulation 1: Standard Elliptic Domain and Dynamic Bumper Domain. In this simulation, we use the standard elliptic domain and the dynamic bumper domain to model the safety zone of the obstacle ship, respectively. Without considering the constraints of the rules and the safe distance for avoidance, the ASV only completes the collision avoidance of obstacle ships through the limitations of (28). Collision avoidance using standard elliptical domains is shown in Figure 9. Figure 10 shows collision avoidance using the dynamic bumper domain. Due to the constraint of (28), when the ASV avoids the obstacle ship, it will prevent the intersection of its safety zone and the safety zone of the obstacle ship. However, it can be seen from Figure 9 that the safety zone of the ASV and the safety zone of the obstacle ship have an intersection, which is caused by the difficulty of the algorithm to calculate the precise distance between the two safety zones in (28). Therefore, we will solve this problem by adding the constraints of the rules and the safe

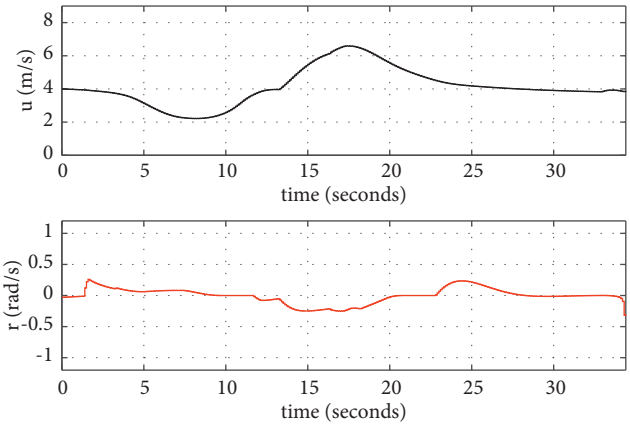

Figure 15: The surge speed and the yaw rate of the ASV during simulation 3.

distance of avoidance in simulations 2–5. It can be seen from Figure 10 : (1) that compared with the standard elliptic domain, the dynamic bumper domain makes the ASV consider a smaller avoidance distance when avoiding the

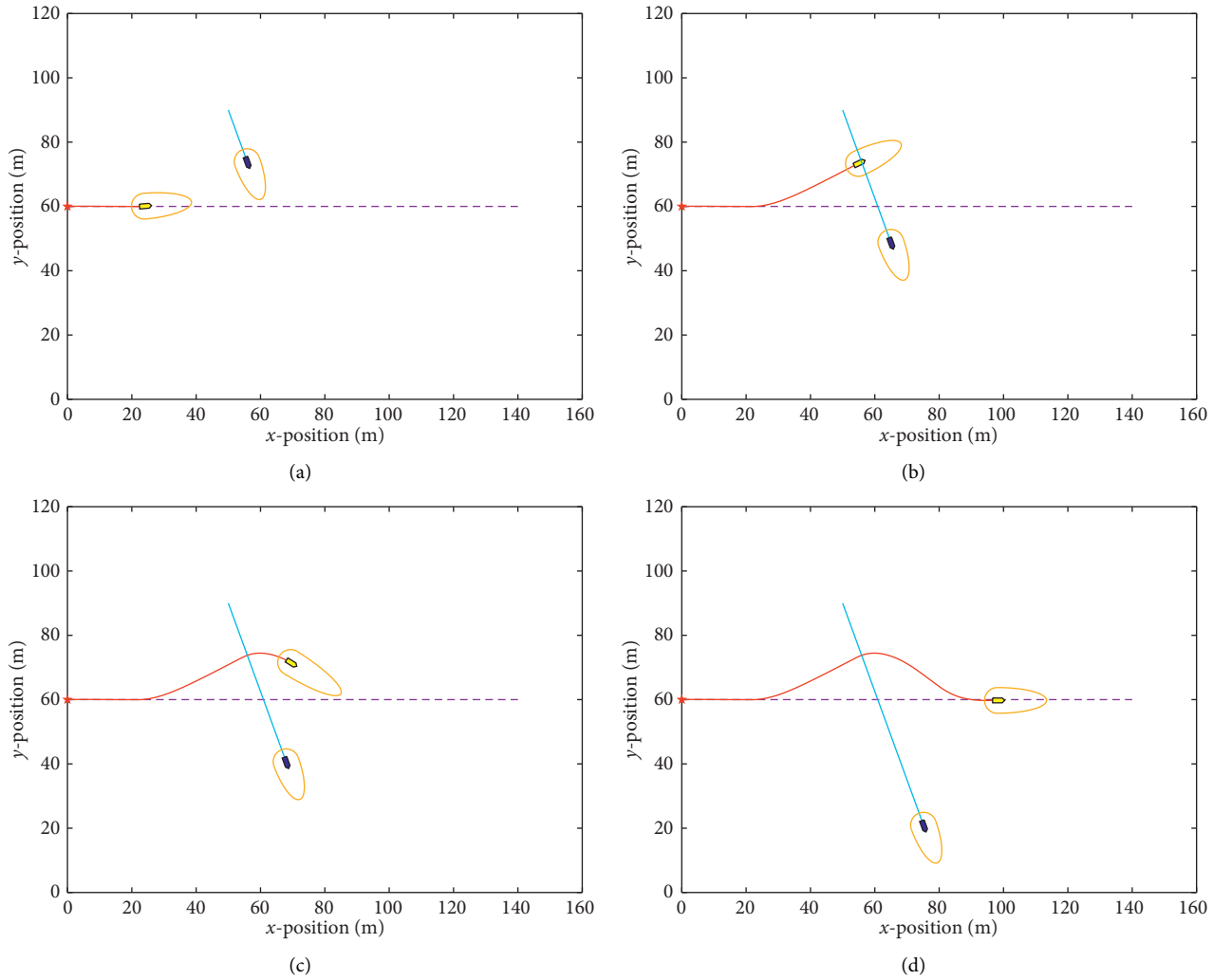

Figure 16: Simulation 4: crossing.

second half of the obstacle ship safety zone, which is more in line with the movement of the ship characteristic. (2) Compared with only using the dynamic bumper safety zone for the obstacle ship, the dynamic bumper safety zone is also used for the ASV. The ASV has a sufficient avoidance distance when avoiding the obstacle, which further ensures the safety of the ASV when avoiding. Therefore, in simulations 2–5, we use the dynamic bumper safety zone for the ASV and obstacle ship. Figure 11 shows the speed change of the ASV when avoiding collision with the obstacle ship using the dynamic bumper domain. It can be seen from Figure 11 that the ASV adopts the evasive maneuver of shifting and steering, and because the distance between the ASV and the obstacle ship is too close for the algorithm to calculate a suitable path through (28) during this period, the ASV has a speed oscillation between 10 and 15 s.

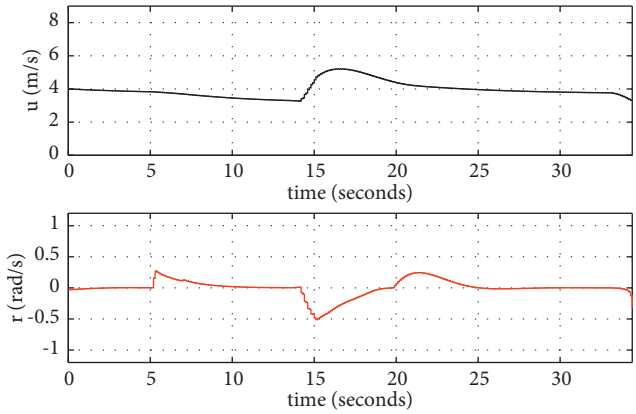

Figure 17: The surge speed and the yaw rate of the ASV during simulation 4.

4.3. Simulation 2: Head-On. In this simulation, we take the relative distance between the ASV and the obstacle ship in the sway direction as the evaluation object of $d_{\text{safe\_heading}}$ in equation (18) so that even if the relative position between the ASV and the obstacle ship rapidly changes, it can be ensured that the ASV has enough reaction time to effectively avoid the obstacle ship. Figure 12 shows the simulation of the head-on encounter. As shown in Figure 12(a), in the beginning, the

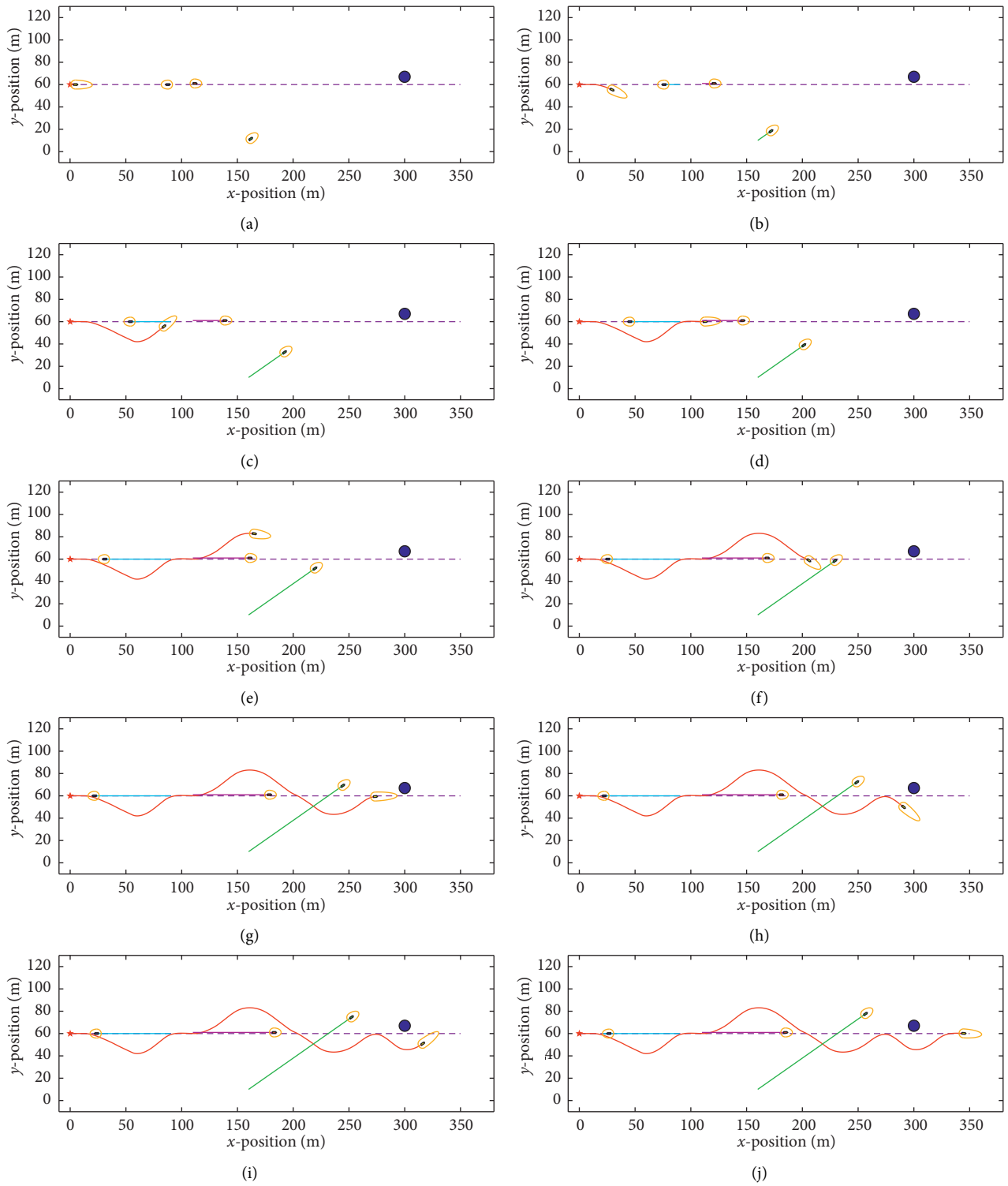

Figure 18: Simulation 5: collision avoidance of static and dynamic obstacles.

obstacle ship directly approached at a constant speed in front of the ASV, and the ASV usually traveled along the given path. As shown in Figure 12(b), when encountering an obstacle ship, the ASV conducted the manipulation of steering to the right and appropriately decelerating to pass the port side of the obstacle ship. The avoidance manipulation met the requirements of Rule 10 of "*RPRCIRCA*." As shown in Figures 12(c) and 12(d), after passing the handicap with the obstacle ship, the ASV manipulated steering to the left and resumed the given path to continue to navigate. Figure 13 displays the changes in the surge speed and the yaw rate of the ASV in the head-on encounter.

4.4. Simulation 3: Overtaking. In this simulation, we assume that the ASV is the overtaking ship and the obstacle ship is overtaken. The Euclidean distance between the ASV and the obstacle ship is selected to evaluate the $d_{safe\_overtaking}$ in equation (19). Figure 14 shows the simulation of the ASV overtaking the obstacle ship. As shown in Figure 14(a), in the beginning, the ASV navigated behind the obstacle ship at the surge speed faster than the obstacle ship along the given path. As shown in Figure 14(b), when starting to overtake the obstacle ship, the ASV first conducted manipulation of appropriately decelerating and steering to the left, and then gradually accelerated to complete the overtaking from the port side of the obstacle ship. The avoidance manipulation met the requirements of Rule 12 of the "*RSRSJSYR*." As shown in Figures 14(c) and 14(d), after passing the obstacle ship, the ASV performed manipulation of steering to the right and accelerating to resume to the given path and continuing to navigate. It can be seen from Figure 14 that, during the overtaking process, the size of the ASV safety zone changed with the ship's velocity, which meets the requirements of algorithm design. Figure 15 shows the change in the surge speed and yaw rate of the ASV during the overtaking process.

4.5. Simulation 4: Crossing. In this simulation, we assume that the ASV is a crossing ship, and the obstacle ship is normally navigating on the navigation lane. The Euclidean distance between the ASV and the obstacle ship is selected as the evaluation of $d_{safe\_crossing}$ in (20). Figure 16 shows the simulation of the ASV crossing the obstacle ship. As shown in Figure 16(a), in the beginning, the obstacle ship approached at a constant surge speed on the left and front of the ASV. As shown in Figure 16(b), when starting to cross the obstacle ship, the ASV first conducted the manipulation of steering to the left and appropriately decelerating, and then gradually accelerated and passed from the stern direction of the obstacle ship. As shown in Figures 16(c) and 16(d), after passing the obstacle ship, the ASV performed manipulation of steering to the right and accelerating to resume to the given path and continuing to navigate. It can be seen from Figure 16 that the avoidance manipulation during the entire crossing process met the requirements of Rule 20 and Rule 28 of "*RSRSJSYR*." Furthermore, no matter where the ASV crossed from the obstacle ship, the collision avoidance algorithm can plan a path that meets the requirements of the rules. Figure 17 displays the change in the surge speed and yaw rate of the ASV during the crossing process.

4.6. Simulation 5: Collision Avoidance of Static and Dynamic Obstacles. In order to fully verify the effectiveness of the proposed algorithm, in this simulation we let ASV avoid collisions for three different encounter situations at the same time. In addition, ASVs need to avoid static obstacles such as river-crossing bridges and buoys when navigating in congested inland waters. In the simulation, such static obstacles were simplified into circular areas with a fixed size, the radius of which varied with the size of the obstacles. Figure 18 shows the simulation of the ASV avoiding collisions with static and dynamic obstacles. As shown in Figure 18(a),

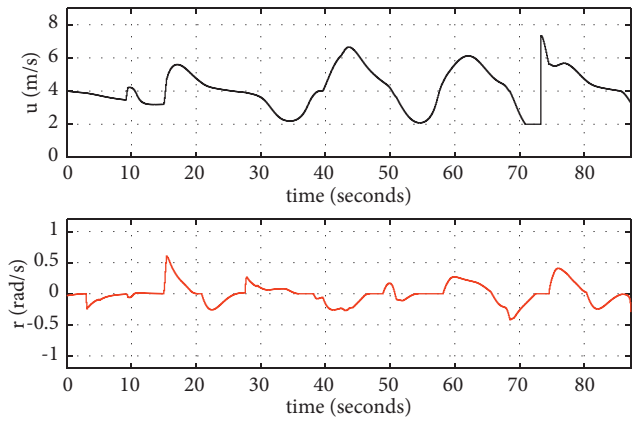

Figure 19: The surge speed and the yaw rate of the ASV during simulation 5.

in the beginning, the ASV follows the reference path from left to right, and the three obstacle ships decelerate along the fixed course, respectively. As shown in Figures 18(b) and 18(c), when the encounter situation with the first obstacle ship (blue) was formed, the ASV first took the evasive maneuver of turning to the right and decelerating. After the first obstacle ship passed the yield, the ASV turned to the left and resumed navigating on the reference path. The entire avoidance process complied with the requirements of Rule 10 of the "RPCIRCA." As shown in Figures 18(d) and 18(e), when the overtaking encounter situation with the second dynamic obstacle ship (purple) was formed, the ASV took a left turn and accelerated maneuver, and overtaking from the left side of the obstacle ship. After overtaking, when passing the obstacle ship, the ASV took a right-hand turn to return to the reference path and continue to navigate. The entire overtaking process complied with the requirements of Rule 12 of the "RSRSJSYR." As shown in Figures 18(f) and 18(g), when the crossing situation was formed with the third obstacle ship (green), the ASV took a right turn and slowed down and passed the stern of the obstacle ship. After giving way, the ASV took the maneuver of turning left and accelerating to resume navigating on the reference path. The entire evasion process complied with the requirements of Rule 20 and Rule 28 of the "RSRSJSYR." As shown in Figures 18(h)–18(j), when the ASV normally follows the reference path, there is a static obstacle in front of the ASV, and the ASV immediately turns to the right and decelerates to avoid the static obstacle. After passing the static obstacle, the ASV took a left turn and resumed navigating on the reference path. Figure 19 shows the change in the surge speed and yaw rate of the ASV during the collision avoidance process.

4.7. Simulation Summary. The proposed algorithm solved all conditions of the encounter while complying with Rules 9–11 of *RPRCIRCA* and Rules 10, 12, 20, and 28 of *RSRSJSYR*. From the process of the ASV avoiding obstacles in simulations 2–5, it can be seen that the ASV has sufficient collision avoidance space to avoid obstacles, and there will be no intersection of the safety zone, as shown in Figure 9.

It can be seen from the speed curve of the ASV in simulations 2–5 that there are some deviations in the speed of the ASV when avoiding collision. Still, the proposed algorithm can effectively compensate for the influence of the current. After adding the avoidance safety distance, the ASV has enough reaction time to avoid the obstacle ship, and the speed of the ASV will not oscillate, as shown in Figure 11 during the collision avoidance process.

The average computation times of the proposed algorithm are 0.0181s in simulation 2, 0.0172s in simulation 3, 0.0192s in simulation 4, and 0.0235s in simulation 5. It can be seen that in all interactive scenarios, the average calculation time of the algorithm is less than 0.025s, which meets the real-time requirements.

5. Conclusions

In this study, an improved collision avoidance algorithm based on model predictive control is proposed to solve the autonomous collision avoidance of ASVs in congested inland waters. The proposed algorithm can comprehensively consider the influence of constraints such as actuators and waterway's boundary and can compensate for current disturbances in real time, which has good robustness. The algorithm adopts the dynamic bumper domain to model the safety zone of the ASV and the obstacle ship. It adopts the maneuvering strategy of reducing the speed and slightly changing the yaw in collision avoidance, which meets the requirements of ASVs in congested inland waters. In the simulation scenarios of head-on, overtaking, crossing, and avoiding collisions against static and dynamic obstacles simultaneously, the proposed algorithm can avoid all collisions, while complying with the rules of *RPRCIRCA* and *RSRSJSYR*. In the future, we will realize the hybrid collision avoidance of ASVs by combining the proposed algorithm with the algorithm of global path planning and comprehensively verifying the algorithm's performance through actual ship experiments.

Data Availability

All data, together with relevant analysis scripts and files, are available from the corresponding author upon request.

Conflicts of Interest

The author declares that there are no conflicts of interest regarding the publication of this paper.

Acknowledgments

This research was funded by the Natural Science Foundation of China (grant no. 51809128) and the Zhenjiang Key R&D Program-Industry Foresight and Common Key Technology Preliminary Guidance Project (grant no. GY2018026).

References

[1] W. Gan, D. Zhu, Z. Hu, X. Shi, L. Yang, and Y. Chen, "Model predictive adaptive constraint tracking control for underwater vehicles," *IEEE Transactions on Industrial Electronics*, vol. 67, no. 9, pp. 7829–7840, 2020.

[2] J. Han, Y. Cho, J. Kim, J. Kim, N. s. Son, and S. Y. Kim, "Autonomous collision detection and avoidance for ARAGON USV: development and field tests," *Journal of Field Robotics*, vol. 37, no. 6, pp. 987–1002, 2020.

[3] H. Huang, J. Tang, and B. Zhang, "Positioning parameter determination based on statistical regression applied to autonomous underwater vehicle," *Applied Sciences*, vol. 11, no. 17, 2021.

[4] Y. Cheng, M. Jiang, J. Zhu, and Y. Liu, "Are we ready for unmanned surface vehicles in inland waterways? The USVInland multisensor dataset and benchmark," *IEEE Robotics and Automation Letters*, vol. 6, no. 2, pp. 3964–3970, 2021.

[5] C. Tam, R. Bucknall, and A. Greig, "Review of collision avoidance and path planning methods for ships in close range encounters," *Journal of Navigation*, vol. 62, no. 3, pp. 455–476, 2009.

[6] T. I. Fossen, *Handbook of Marine Craft Hydrodynamics and Motion Control*, John Wiley & Sons, Chichester, UK, 2011.

[7] A. Vagale, R. Oucheikh, R. T. Bye, O. L. Osen, and T. I. Fossen, "Path planning and collision avoidance for autonomous surface vehicles I: a review," *Journal of Marine Science and Technology*, vol. 26, no. 4, pp. 1292–1306, 2021.

[8] M. Hoy, A. S. Matveev, and A. V. Savkin, "Algorithms for collision-free navigation of mobile robots in complex cluttered environments: a survey," *Robotica*, vol. 33, no. 3, pp. 463–497, 2015.

[9] B. H. Eriksen, E. F. Wilthil, A. L. Flåten, E. F. Brekke, and M. Breivik, "Radar-based maritime collision avoidance using dynamic window," in *Proceedings of the IEEE Aerospace Conference*, pp. 1–9, Big Sky, MT, USA, March 2018.

[10] C. Wang, Y. S. Mao, K. J. Du, B. Hu, and L. F. Song, "Simulation on local obstacle avoidance algorithm for unmanned surface vehicle," *International Journal of Simulation Modelling*, vol. 15, no. 3, pp. 460–472, 2016.

[11] D. Fox, W. Burgard, and S. Thrun, "The dynamic window approach to collision avoidance," *IEEE Robotics and Automation Magazine*, vol. 4, no. 1, pp. 23–33, 1997.

[12] O. Khatib, "Real-Time obstacle avoidance for manipulators and mobile robots," in *Proceedings of the 1985 IEEE International Conference on Robotics and Automation*, pp. 500–505, St. Louis, MO, USA, March 1985.

[13] J. Song and J. Su, "Path planning for unmanned surface vehicle based on predictive artificial potential field," *International Journal of Advanced Robotic Systems*, vol. 17, pp. 1–13, 2020.

[14] G. Xia, Z. Han, B. Zhao, and X. Wang, "Local path planning for unmanned surface vehicle collision avoidance based on modified quantum particle swarm optimization," *Complexity*, vol. 2020, Article ID 3095426, 15 pages, 2020.

[15] P. Fiorini and Z. Shiller, "Motion planning in dynamic environments using velocity obstacles," *The International Journal of Robotics Research*, vol. 17, no. 7, pp. 760–772, 1998.

[16] M. Abdelaal, M. Fränzle, and A. Hahn, "NMPC-based trajectory tracking and collison avoidance of underactuated vessels with elliptical ship Domain**This research is supported by the state of lower saxony as part of the project critical systems engineering for socio-technical systems (CSE)," *IFAC-PapersOnLine*, vol. 49, no. 23, pp. 22–27, 2016.

[17] I. B. Hagen, D. K. M. Kufoalor, E. F. Brekke, and T. A. Johansen, "MPC-based collision avoidance strategy for existing marine vessel guidance systems," in *Proceedings of the 2018 IEEE International Conference on Robotics and Automation*, pp. 7618–7623, Brisbane, QLD, Australia, May 2018.

[18] W. Li, "Path following method research for unmanned surface vessels based on predictive control," Master's Thesis, Harbin Engineering University, Harbin, China, 2015.
[19] T. A. Johansen, T. Perez, and A. Cristofaro, "Ship collision avoidance and COLREGS compliance using simulation-based control behavior selection with predictive hazard assessment," *IEEE Transactions on Intelligent Transportation Systems*, vol. 17, no. 12, pp. 3407–3422, 2016.
[20] B. Lei, L. Wu, and Z. Lin, "Harmonic current suppression of dual three-phase PMSM based on model predictive direct torque control," *Mathematical Problems in Engineering*, vol. 2021, Article ID 3043673, 10 pages, 2021.
[21] B. Lindqvist, S. S. Mansouri, A. Agha-mohammadi, and G. Nikolakopoulos, "Nonlinear MPC for collision avoidance and control of UAVs with dynamic obstacles," *IEEE Robotics and Automation Letters*, vol. 5, no. 4, pp. 6001–6008, 2020.
[22] S. Chen, G. Xiong, H. Chen, and D. Negrut, "MPC-based path tracking with PID speed control for high-speed autonomous vehicles considering time-optimal travel," *Journal of Central South University*, vol. 27, no. 12, pp. 3702–3720, 2020.
[23] S. Dixit, U. Montanaro, M. Dianati et al., "Trajectory planning for autonomous high-speed overtaking in structured environments using robust MPC," *IEEE Transactions on Intelligent Transportation Systems*, vol. 21, no. 6, pp. 2310–2323, 2020.
[24] R. Mao, H. Gao, and L. Guo, "A novel collision-free navigation approach for multiple nonholonomic robots based on ORCA and linear MPC," *Mathematical Problems in Engineering*, vol. 2020, Article ID 4183427, 16 pages, 2020.
[25] X. Sun, G. Wang, Y. Fan, D. Mu, and B. Qiu, "Collision avoidance using finite control set model predictive control for unmanned surface vehicle," *Applied Sciences*, vol. 8, no. 6, 2018.
[26] B. H. Eriksen, G. Bitar, M. Breivik, and A. M. Lekkas, "Hybrid collision avoidance for ASV compliant with COLREGs rules 8 and 13-17," *Frontiers in Robotics and AI*, vol. 7, no. 11, pp. 1–18, 2020.
[27] X. Sun, G. Wang, Y. Fan, D. Mu, and B. Qiu, "Collision avoidance of podded propulsion unmanned surface vehicle with COLREGs compliance and its modeling and identification," *IEEE Access*, vol. 6, pp. 55473–55491, 2018.
[28] X. Cheng, "Trajectory optimization for inland waterway ship," *Journal of Wuhan University of Technology*, vol. 30, pp. 576–578, 2018.
[29] J. Zhang, *Velocity Obstacle-Based Algorithm of Collision Avoidance of River Ferry*, Master's Thesis, Dalian Maritime University, Dalian, China, 2018.
[30] H. Shen, *Collision Avoidance Navigation and Control for Unmanned Marine Vessels Based on Reinforcement Learning*, Doctoral Thesis, Dalian Maritime University, Dalian, China, 2018.
[31] K. Hara, "Proposal of maneuvering standard to avoid collision in congested sea area," *Journal of Japan Institute of Navigation*, vol. 85, pp. 33–40, 1991.
[32] C. Tam and R. Bucknall, "Collision risk assessment for ships," *Journal of Marine Science and Technology*, vol. 15, no. 3, pp. 257–270, 2010.
[33] J. Bi, *The Study on Inland Vessel Automatic Collision Avoidance Decision*, Master's thesis, Dalian Maritime University, Dalian, China, 2016.
[34] K. Worthmann, M. W. Mehrez, M. Zanon, G. K. I. Mann, R. G. Gosine, and M. Diehl, "Model predictive control of nonholonomic mobile robots without stabilizing constraints and costs," *IEEE Transactions on Control Systems Technology*, vol. 24, no. 4, pp. 1394–1406, 2016.